

Article

Improved Solubility of Vortioxetine Using C2-C4 Straight-Chain Dicarboxylic Acid Salt Hydrates

Lei Gao, Xian-Rui Zhang *, Shao-Ping Yang, Juan-Juan Liu and Chao-Jie Chen

School of Chemical Engineering and Resource Recycling, Wuzhou University, Wuzhou 543000, China; gaolei_1008@163.com (L.G.); ysp1120@163.com (S.-P.Y.); jjliu2017@163.com (J.-J.L.); chenchaojie@fjmu.edu.cn (C.-J.C.)

* Correspondence: zhangyang159246@163.com; Tel.: +86-0774-582-8709

Received: 5 August 2018; Accepted: 31 August 2018; Published: 2 September 2018



Abstract: The purpose of this study was to improve the solubility of vortioxetine by crystal engineering principles. In this paper, three C2-C4 straight-chain dicarboxylic acid salt hydrates of vortioxetine (VOT-OA, VOT-MA-H₂O, and VOT-SUA-H₂O, VOT = vortioxetine, OA = Oxalic acid, MA = malonic acid, SUA = succinic acid) were synthesized and characterized by single X-ray diffraction, powder X-ray diffraction, and differential scanning calorimetry. The single crystal structure of three salts reveals that vortioxetine has torsional flexibility, which can encourage VOT to allow combination with aliphatic dicarboxylic acids through N⁺-H...O hydrogen bonds. The solubility of all salts exhibits a dramatic increase in distilled water, especially for VOT-MA-H₂O salt, where it shows the highest solubility, by 96-fold higher compared with pure vortioxetine.

Keywords: vortioxetine; dicarboxylic acid; salt hydrates; crystal structure

1. Introduction

During the past decades, a lot of active pharmaceutical ingredients (APIs) have failed at the preclinical stage due to their poor physicochemical properties, especially due to problems related to low solubility, which usually have an effect on GI absorption [1–4]. Crystal engineering provides one straight way to improve the solubility and bioavailability of poorly soluble drugs without disturbing the inherent pharmacological properties of APIs [5–10]. This is especially true for drug salt or drug salt hydrate formation, which can usually improve the solubility of poorly soluble drugs. For example, there have been many researches on the significant solubility improvement of such drugs by forming cocrystals or salts with oxalic acid, malonic acid, and succinic acid [11–15].

Vortioxetine (VOT) is a novel antidepressant, an active pharmaceutical ingredient, which is used for the treatment of major depressive disorder [16]. VOT is a poorly water-soluble drug (0.04 mg mL⁻¹) [17], and it was commercialized in a hydrobromide salt form. To date, there are several literatures [17–20] on 14 salts of VOT (with hydrobromic acid, hydrochloric acid, *p*-hydroxybenzoic acid, saccharin, L-aspartic acid, *p*-toluic acid, *p*-nitrobenzoic acid, *p*-aminobenzoic acid, salicylic acid, 5-fluorouracil, and (*p*-nitrophenyl)-acetic acid). Of these, the salt with L-aspartic acid could remarkably increase the solubility of VOT, which indicates that dicarboxylic acids might have a huge potential in improving the solubility of VOT. The purpose of this study was to improve the aqueous solubility of the drug via crystallization with dicarboxylic acids. In this paper, three C2-C4 straight-chain dicarboxylic acid salt hydrates of vortioxetine were obtained by slow solvent evaporation crystallization with dicarboxylic acid (oxalic acid, malonic acid and succinic acid). Among these salts, succinic acid is a GRAS (Generally Regarded as Safe) compound. The chemical structures of VOT and cofomers are displayed in Figure 1.

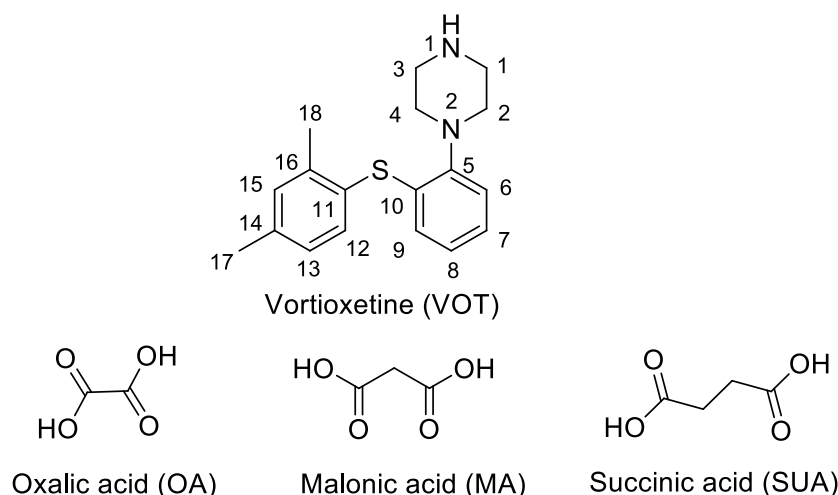


Figure 1. Chemical structures of VOT and coformers.

2. Materials and Methods

2.1. Materials and General Methods

All solvents and reagents (analytical grade) were obtained commercially and used as received unless otherwise mentioned. Differential scanning calorimetry (DSC) studies were carried out using a Mettler-Toledo DSC with a heating regime of 10 °C/min under a nitrogen gas purge. Thermogravimetric analysis (TGA) was performed in a Perkin-Elmer TGA 4000 equipment with a heating rate of 10 °C/min under a nitrogen gas purge. Powder X-ray diffraction (PXRD) patterns were obtained with a German Bruker corporation D8 ADVANCE powder diffractometer coupled with a Cu K α radiation tube ($\lambda = 1.5418 \text{ \AA}$, $V = 40 \text{ kV}$ and $I = 40 \text{ mA}$) and 2θ scan in the 3–60° range.

2.2. Synthesis of VOT-OA Salt (1:1)

VOT-OA salt was obtained by dissolving VOT (20 mg) and OA (6 mg) in 8 mL of acetone-water mixed solvents (3:1, v/v), and stirred at room temperature for 2 h. The resulting solution was left for slow evaporation. The fine block crystals suitable for crystal X-ray diffraction were obtained after 15 days.

2.3. Synthesis of VOT-MA-H₂O Salt (1:1:1)

VOT-MA-H₂O salt was obtained by dissolving VOT (20 mg) and MA (7 mg) in 4 mL of acetone-toluene mixed solvents (1:1, v/v), and stirred at room temperature for 2 h. The resulting solution was left for slow evaporation at an about 35% humidity environment. The fine block crystals suitable for crystal X-ray diffraction were obtained after 15 days.

2.4. Synthesis of VOT-SUA-H₂O Salt (1:1:0.5)

VOT-SUA-H₂O salt was obtained by dissolving VOT (20 mg) and SUA (8 mg) in 6 mL of methanol-water mixed solvents (2:1, v/v), and stirred at room temperature for 2 h. The resulting solution was left for slow evaporation. Fine needlelike crystals suitable for single crystal X-ray diffraction were obtained after 12 days. All VOT salts can also be obtained upon acetonitrile liquid-assisted grinding methods.

2.5. X-ray Crystallography

All the crystal structures were collected on a Bruker Apex II CCD diffractometer operating at 50 kV and 30 mA using Mo K α radiation ($\lambda = 0.71073 \text{ \AA}$). All crystal structures were solved with direct methods using SHELXS-97 [21–23]. The final refinements were performed by full-matrix least-squares

methods with anisotropic thermal parameters for all non-hydrogen atoms on F^2 . The hydrogen atoms on non-carbon atoms were located in difference electron density maps, and the hydrogen atoms riding on the carbon atoms were geometrically fixed using theoretical calculation and were refined isotropically. Crystallographic parameters and hydrogen bonds are listed in Tables 1 and 2.

Table 1. Crystallographic Parameters of Vortioxetine and its dihydroxybenzoic acid salts.

	VOT-OA	VOT-MA-H ₂ O	VOT-SUA-H ₂ O
chemical formula	C ₁₈ H ₂₃ N ₂ S, C ₂ HO ₄	C ₁₈ H ₂₃ N ₂ S, C ₃ H ₃ O ₄ , H ₂ O	C ₁₈ H ₂₃ N ₂ S, C ₄ H ₅ O ₄ , 1/2H ₂ O
formula sum	C ₂₀ H ₂₄ N ₂ O ₄ S	C ₂₁ H ₂₈ N ₂ O ₅ S	C ₂₂ H ₂₉ N ₂ O _{4.5} S
formula weight	388.47	420.51	425.53
crystal system	triclinic	monoclinic	monoclinic
space group	<i>P</i> 1̄	<i>P</i> 2 ₁ / <i>n</i>	<i>C</i> 2/ <i>c</i>
<i>a</i> [Å]	5.7423(4)	17.550(3)	39.091(8)
<i>b</i> [Å]	6.7539(5)	7.4423(11)	6.5734(13)
<i>c</i> [Å]	26.162(2)	18.120(4)	18.601(4)
α [°]	96.730(6)	90	90
β [°]	91.712(6)	109.20(2)	112.55(3)
γ [°]	105.756(7)	90	90
<i>Z</i>	2	4	8
<i>V</i> [Å ³]	967.77(12)	2234.0(7)	4414.3(15)
<i>D</i> _{calc} [g cm ⁻³]	1.333	1.250	1.281
<i>M</i> [mm ⁻¹]	0.196	0.178	0.179
reflns. collected	8330	8633	8096
unique reflns.	2178	2688	1824
observed reflns.	3378	3935	4208
<i>R</i> ₁ [<i>I</i> > 2σ(<i>I</i>)]	0.0511	0.0495	0.0691
<i>wR</i> ₂ (all data, <i>F</i> ²)	0.1191	0.1317	0.1112
GOF	1.004	1.048	0.975
largest diff. peak and hole [e·Å ⁻³]	0.190/−0.230	0.225/−0.234	0.213/−0.236
CCDC	1860303	1860304	1860305

Table 2. Hydrogen bond distances (Å) and angles (°) for three salt hydrates.

Compound	D-H...A	d(D-H)	d(H...A)	d(D...A)	<(DHA)	Symmetry Code
VOT-OA	N1 ⁺ -H1A...O4	0.95	1.84	2.760(4)	160	− <i>x</i> + 1, − <i>y</i> + 1, − <i>z</i> + 1
	N1 ⁺ -H1B...O3	0.98	1.93	2.809(4)	147	<i>x</i> , <i>y</i> + 1, <i>z</i>
	O2-H2...O3	0.97	1.61	2.582(4)	173	<i>x</i> + 1, <i>y</i> , <i>z</i>
VOT-MA-H ₂ O	N1 ⁺ -H1A...O5	0.96	1.77	2.717(3)	171	− <i>x</i> + 1/2, <i>y</i> − 1/2, − <i>z</i> + 1/2
	N1 ⁺ -H1B...O2	0.91	1.88	2.785(3)	173	<i>x</i> , <i>y</i> − 1, <i>z</i>
	N1 ⁺ -H1B...O4	0.91	2.45	3.094(3)	127	<i>x</i> , <i>y</i> − 1, <i>z</i>
	O5-H5A...O1	0.83	1.90	2.717(3)	168	− <i>x</i> + 1, − <i>y</i> + 1, − <i>z</i> + 1
	O5-H5B...O2	1.00	1.73	2.731(3)	170	<i>x</i> + 1, <i>y</i> , <i>z</i>
VOT-SUA-H ₂ O	O3-H3...O4	0.96	1.53	2.443(3)	155	<i>x</i> , <i>y</i> , <i>z</i>
	N1 ⁺ -H1A...O1	0.99	1.79	2.730(4)	158	<i>x</i> , <i>y</i> , <i>z</i>
	N1 ⁺ -H1A...O5	0.86	1.90	2.756(4)	172	<i>x</i> , <i>y</i> , <i>z</i>
	O2-H2...O3	0.87	1.57	2.443(4)	174	<i>x</i> , <i>y</i> − 1, <i>z</i>
	O5-H5A...O4	0.89	1.80	2.691(4)	170	<i>x</i> , − <i>y</i> + 2, <i>z</i> − 1/2

2.6. Solubility Measurement

Equilibrium solubility experiments were measured in a round bottomed flask at 37 ± 0.5 °C in aqueous medium. In a typical experiment, 25 mL of aqueous medium was added to a round bottomed flask containing 250 mg of solid samples and rotated at 500 rpm. After 24 h the resulting solution was filtered with 0.22 μm nylon filter and then diluted by aqueous medium. The concentration of VOT was assayed using an Agilent 1290 HPLC system, with a C18 HPLC column (Thermo Accucore aQ 100 × 2.1 mm) and an UV detection wavelength of 226 nm. The column temperature was set at 40 °C, and the mobile phase containing of 0.01 mol/L potassium phosphate: acetonitrile (*v/v*, 60:40) was run at 0.4 mL/min. The powder dissolution study was also determined using the Agilent 1290 HPLC system, and all of the solids were milled to powder and sieved using standard mesh sieves with

approximate size ranges of 140–250 μm . At a regular interval of 15–30 min, 2.5 mL of dissolution samples were successively collected and replaced by equal volume of fresh medium to maintain a constant volume. All of the resulting solution was filtered with 0.22 μm nylon filter and analyzed by the corresponding calibration curve. The HPLC graphs of VOT and its salts are shown in Figure S1.

3. Results and Discussion

3.1. Crystal Structure Analysis

3.1.1. VOT-OA (1:1) Salt

The VOT-OA salt crystallized in the triclinic $P\bar{1}$ space group with one protonated VOT cation and one deprotonated OA anion in the asymmetric unit. As shown in Figure 2a, two VOT cations and two OA anions interact through $\text{N1}^+-\text{H1A}\cdots\text{O4}$ and $\text{N1}^+-\text{H1B}\cdots\text{O3}$ hydrogen bonds, in a tetrameric $R_4^4(12)$ motif. These adjacent tetramers form a one-dimensional chain structure through $\text{O2}-\text{H2}\cdots\text{O3}$ hydrogen bonds (Figure 2b).

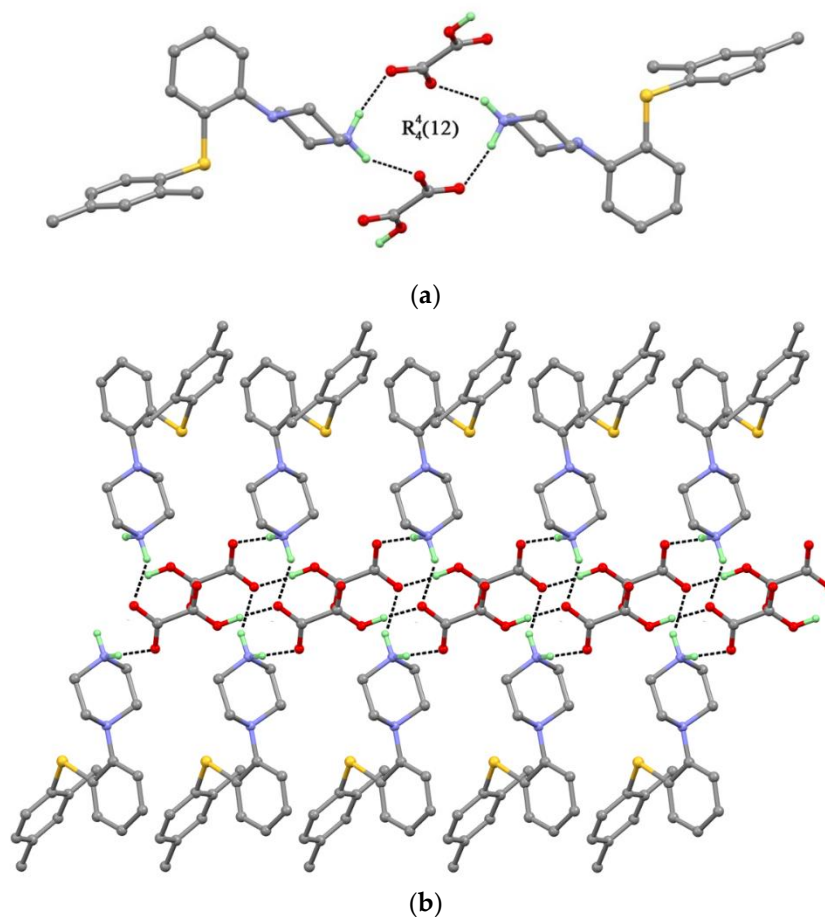


Figure 2. (a) Inversion related VOT-OA salt molecules connected by $\text{N}^+-\text{H}\cdots\text{O}$ hydrogen bonds in a tetrameric $R_4^4(12)$ motif; (b) The sandwich layer structure is connected by $\text{O}-\text{H}\cdots\text{O}$ hydrogen bonds.

3.1.2. VOT-MA-H₂O (1:1:1) Salt

The VOT-MA-H₂O salt crystallized in the monoclinic $P21/n$ space group with one protonated VOT cation, one deprotonated MA anion, and one water molecule in the asymmetric unit. In the molecular structure, two MA anions and two water molecules form a tetrameric $R_4^4(16)$ motif through $\text{O5}-\text{H5A}\cdots\text{O1}$ and $\text{O5}-\text{H5B}\cdots\text{O2}$ hydrogen bonds (Figure 3a). These tetramers are connected

to four adjacent VOT cations via $N1^+-H1A\cdots O5$ and $N1^+-H1B\cdots O2$ hydrogen bonds, forming a two-dimensional supramolecular network (Figure 3b).

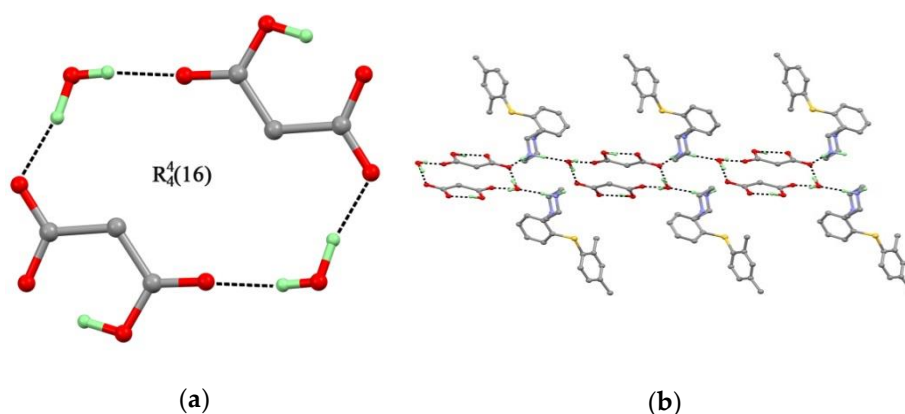


Figure 3. (a) Two MA anions and two water molecules form a tetrameric $R_4^4(16)$ motif through $O5-H5A\cdots O1$ and $O5-H5B\cdots O2$ hydrogen bonds; (b) The two-dimensional structure is connected by $N1^+-H1A\cdots O5$ and $N1^+-H1B\cdots O2$ hydrogen bonds.

3.1.3. VOT-SUA-H₂O (1:1:0.5) Salt

The VOT-SUA-H₂O salt crystallized in the monoclinic $C2/c$ space group with one protonated VOT cation, one deprotonated SUA anion, and one half water molecule in the asymmetric unit. In the molecular structure, two SUA anions and one water molecule form a two-dimensional sheet-like structure through $O5-H5A\cdots O4$ and $O2-H2\cdots O3$ hydrogen bonds (Figure 4a), and these sheet-like structures are connected to the corresponding VOT cations via $N1^+-H1A\cdots O1$ and $N1^+-H1B\cdots O5$ hydrogen bonds, forming a $R_6^6(22)$ motif (Figure 4b).

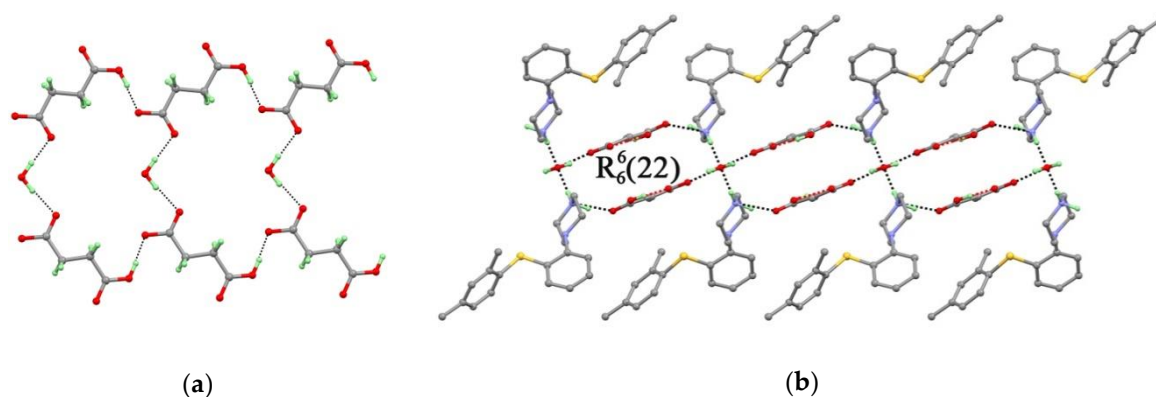


Figure 4. (a) Two SUA anions and one water molecules form a sheet-like structure through $O5-H5A\cdots O4$ and $O2-H2\cdots O3$ hydrogen bonds; (b) The $R_6^6(22)$ motif structure are connected by $N1^+-H1A\cdots O1$ and $N1^+-H1B\cdots O5$ hydrogen bonds.

3.1.4. Conformational Flexibility

The conformation flexibility of the drug is very important in matching the requirement of configuration through hydrogen bonding with different conformers [24–26]. In fact, the three planes (C5-C6-C7-C8-C9-C10 (A), C10-S1-C11 (B), and C5-N2-N1 (C)) of VOT had torsional flexibility, and the selected torsional angles are listed in Table S1. In the following comparison, the A-planes of these flexible molecules are fixed and used as reference plane. Variable conformational of VOT in these

4 crystals are compared with each other and shown in Figure 5, and the torsional angles variation between A-B and A-C are in the ranges of $4.6(4)$ – $18.3(4)^\circ$ and $20.9(4)$ – $43.8(3)^\circ$, respectively.

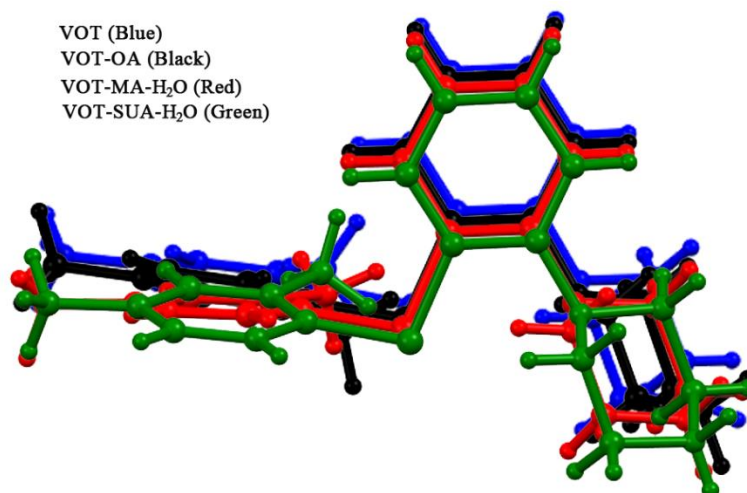


Figure 5. Overlay of VOT molecules extracted from crystal structures. Color codes: blue = VOT; black = VOT-OA (1:1); red = VOT-MA-H₂O (1:1:1); green = VOT-SUA-H₂O (1:1:0.5).

3.2. Powder X-ray Diffraction

The experimental PXRD patterns for VOT, VOT-OA, VOT-MA-H₂O, and VOT-SUA-H₂O salt are shown in Figure 6. The results showed that the PXRD patterns matched well with the calculated patterns from the crystal data, which indicated the excellent phase purity of solid samples.

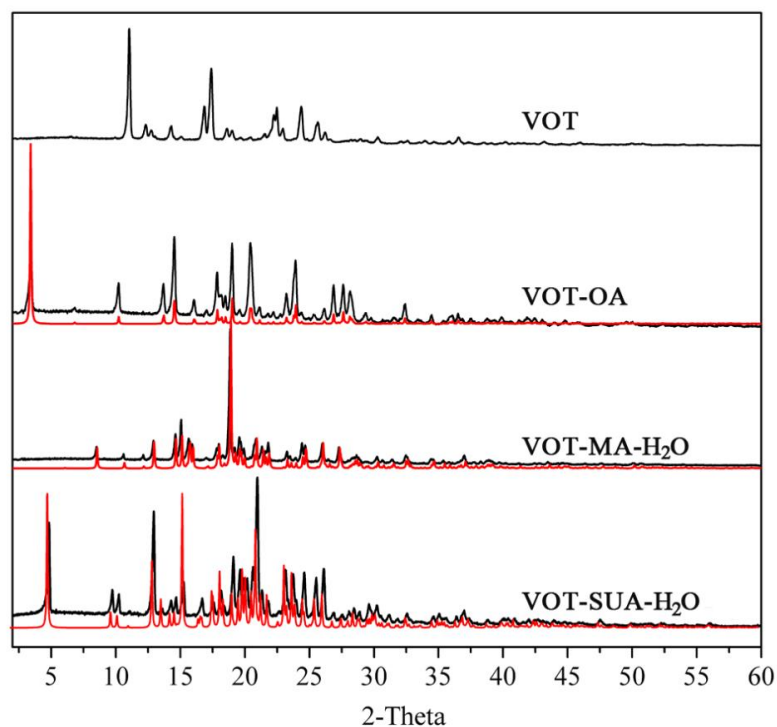


Figure 6. Experimental (black) and simulated (red) powder X-ray diffraction patterns for VOT, VOT-OA, VOT-MA-H₂O, and VOT-SUA-H₂O salt.

3.3. Thermal Analysis

All vortioxetine salts are investigated by DSC and TGA under a nitrogen gas atmosphere. The DSC and TGA profiles of VOT and its salts were shown in Figure 7 and Figure S2. The DSC thermogram of pure VOT exhibits a single melting endothermic peak at 117 °C attributed to the melting process. The TGA curve shows that VOT has no weight loss before decomposition at 226 °C.

The DSC thermogram of VOT-OA shows endothermic peak at 208 °C and 218 °C, indicating that a phase transition begins to happen after melting. The TGA curve shows that VOT-OA has no weight loss before decomposition at 207 °C.

The DSC thermogram of VOT-MA-H₂O displays a two-step endothermic transition between 70 and 112 °C accompanied by a mass loss of 4.22% (theoretical value: 4.28%) in the TGA curve, suggesting the loss of water molecules from the crystal structure. The next endothermic peak at 132 °C and 159 °C corresponds to the decomposition that begins to happen after melting.

The phenomenon is also observed in VOT-SUA-H₂O salt, the DSC thermogram of VOT-SUA-H₂O shows a two-step endothermic peak at 50 and 140 °C associated with a mass loss of 2.04% (theoretical value: 2.12%) in the TGA curve, corresponding to the loss of half a water molecule, and the latter endothermic peak at 144 °C, indicating that the decomposition begins to happen after melting.

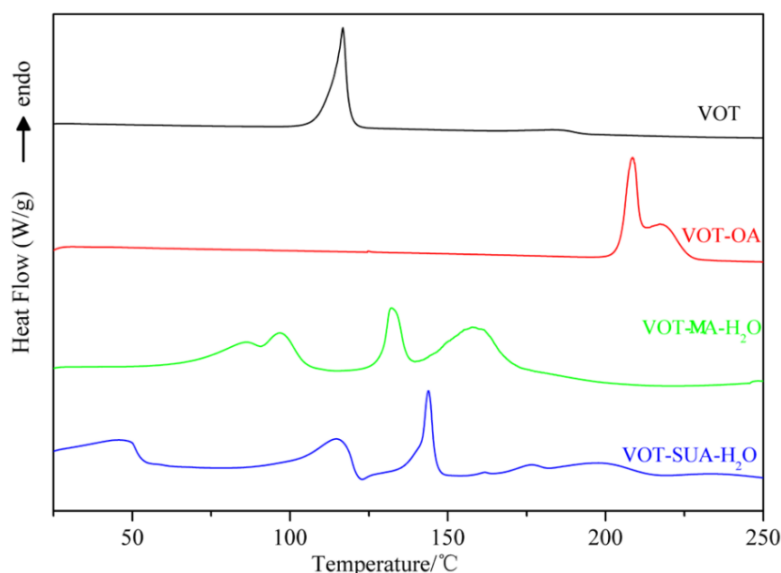


Figure 7. DSC thermograms of VOT, VOT-OA, VOT-MA-H₂O, and VOT-SUA-H₂O salt.

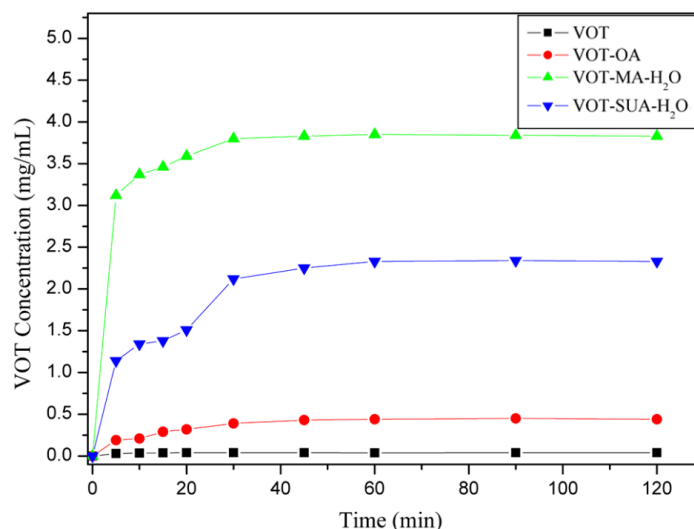
3.4. Solubility and Powder Dissolution Rate Analysis

Equilibrium solubility experiments for VOT and its salts are performed in a water medium at 37 °C. As shown in Table 3, all salts display an improvement in the solubility compared to pure VOT. Specifically, VOT-MA-H₂O (1:1:1) salt shows 96-fold higher solubility compared to pure vortioxetine. The solubility order in aqueous medium is the following, VOT-MA-H₂O > VOT-SUA-H₂O > VOT-OA > VOT. The rule may be interpreted according to the solubility ability of coformers. Salt solubility is directly associated with the solubility of the coformer, which indicates that more soluble coformers lead to more soluble salts [12]. The powder samples of the undissolved residue are also analyzed via PXRD, the result shows that all VOT salts remained stable in water at 37 °C after 24 h solubility experiments (Figures S3–S5).

The powder dissolution profiles of VOT, VOT-OA, VOT-MA-H₂O, and VOT-SUA-H₂O salts in water are shown in Figure 8. The maximum values of VOT concentrations of VOT-OA, VOT-MA-H₂O, and VOT-SUA-H₂O salts were approximately 11, 104, and 58 times larger than that of pure VOT, respectively. Further, the powder dissolution studied indicates that the VOT-MA-H₂O and VOT-SUA-H₂O salts have a better powder dissolution property that can be a promising drug candidate.

Table 3. Powder solubility test results ($n = 3$).

Sample in Water	Solubility of API (mg/mL)	pH in Water after 24 h Slurry	Coformer Solubility (mg/mL) [27]
Pure vortioxetine	0.04	7.62	-
VOT-OA	0.44 ($\times 11$)	5.43	124
VOT-MA-H ₂ O	3.84 ($\times 96$)	5.90	623
VOT-SUA-H ₂ O	2.33 ($\times 58$)	6.24	135

**Figure 8.** Powder dissolution profiles of VOT, VOT-OA, VOT-MA-H₂O, and VOT-SUA-H₂O salts at different time points in pure water at 37 °C.

4. Conclusions

In summary, three C2-C4 straight-chain dicarboxylic acid salt hydrates of vortioxetine (VOT-OA, VOT-MA-H₂O, and VOT-SUA-H₂O) were prepared and characterized through slow solvent evaporation crystallization in this paper. The single crystal structure of the three salts reveals that vortioxetine has torsional flexibility, which can encourage VOT to allow combination with aliphatic dicarboxylic acids through N⁺-H...O hydrogen bonds. Comparison of the solubility values suggests that the VOT-MA-H₂O (1:1:1) salt and VOT-SUA-H₂O (1:1:0.5) salt show higher solubility compared with pure vortioxetine. Thus, both VOT-MA-H₂O (1:1:1) salt and VOT-SUA-H₂O (1:1:0.5) salt are promising drug candidates for the further development of VOT formulation. However, preclinical studies should be conducted to investigate VOT-MA-H₂O (1:1:1) and VOT-SUA-H₂O (1:1:0.5) salt's bioavailability and toxicity before formulation.

Supplementary Materials: The following are available online at <http://www.mdpi.com/2073-4352/8/9/352/s1>, Figure S1: The HPLC graphs of VOT and its salts; Figure S2: The TGA plots of VOT and its salts; Figure S3: Comparison PXRD patterns of VOT-OA and its residual materials after 24 h solubility in aqueous medium; Figure S4: Comparison PXRD patterns of VOT-MA-H₂O and its residual materials after 24 h solubility in aqueous medium; Figure S5: Comparison PXRD patterns of VOT-SUA-H₂O and its residual materials after 24 h solubility in aqueous medium; Table S1: Torsion angles (°) variation of VOT molecules extracted from crystal structures; Table S2: Preparation of VOT salts.

Author Contributions: L.G. and X.-R.Z. conceived and designed the experiments; S.-P.Y. and J.-J.L. performed the experiments and analyzed the data; C.-J.C. supervised the work. All the authors have contributed to manuscript revision.

Funding: This research was funded by Fujian Natural Science Foundation (Grant No.: 2017J01443) and Wuzhou University Foundation (Grant No.: 2017A003 and 2017B015).

Acknowledgments: The work was supported by Fujian Natural Science Foundation (Grant No.: 2017J01443) and Wuzhou University Foundation (Grant No.: 2017A003 and 2017B015).

Conflicts of Interest: The authors declare no conflict of interest.

References

1. Prohotsky, D.L.; Zhao, F. A survey of top 200 drugs—inconsistent practice of drug strength expression for drugs containing salt forms. *J. Pharm. Sci.* **2012**, *101*, 1–6. [[CrossRef](#)] [[PubMed](#)]
2. Thayer, A.M. Form and function. *Chem. Eng. News* **2007**, *85*, 17–30. [[CrossRef](#)]
3. Kola, I.; Landis, J. Can the pharmaceutical industry reduce attrition rates? *Nat. Rev. Drug Discov.* **2004**, *3*, 711–716. [[CrossRef](#)] [[PubMed](#)]
4. Mittapalli, S.; Mannava, M.C.; Khandavilli, U.R.; Allu, S.; Nangia, A. Soluble salts and cocrystals of clotrimazole. *Cryst. Growth Des.* **2015**, *15*, 2493–2504. [[CrossRef](#)]
5. Chen, X.; Li, D.; Luo, C.; Wang, J.; Deng, Z.; Zhang, H. Cocrystal of zileuton with enhanced physical stability. *CrystEngComm* **2018**, *20*, 990–1000. [[CrossRef](#)]
6. Silva Filho, S.F.; Pereira, A.C.; Sarraguca, J.M.; Sarraguca, M.C.; Lopes, J.; Freitas Filho, P.; dos Santos, A.O.; da Silva Ribeiro, R.R. Synthesis of a glibenclamide cocrystal: Full spectroscopic and thermal characterization. *J. Pharm. Sci.* **2018**, *107*, 1597–1604. [[CrossRef](#)] [[PubMed](#)]
7. Shimpi, M.R.; Alhayali, A.; Cavanagh, K.L.; Rodriguez-Hornedo, N.; Velaga, S.P. Tadalafil-malonic acid cocrystal: Physicochemical characterization, pH-solubility, and supersaturation studies. *Cryst. Growth Des.* **2018**, *8*, 4378–4387. [[CrossRef](#)]
8. Sa, R.; Zhang, Y.; Deng, Y.; Huang, Y.; Zhang, M.; Lou, B. Novel salt cocrystal of chrysin with berberine: Preparation, characterization, and oral bioavailability. *Cryst. Growth Des.* **2018**, *18*, 4724–4730. [[CrossRef](#)]
9. Mondal, P.K.; Rao, V.; Mittapalli, S.; Chopra, D. Exploring solid state diversity and solution characteristics in a fluorine-containing drug riluzole. *Cryst. Growth Des.* **2017**, *17*, 1938–1946. [[CrossRef](#)]
10. An, J.H.; Lim, C.; Ryu, H.C.; Kim, J.S.; Kiyonga, A.N.; Park, M.; Suh, Y.G.; Park, G.H.; Jung, K. Structural characterization of febuxostat/L-pyroglutamic acid cocrystal using solid-state ¹³C-NMR and investigation study of its water solubility. *Crystals* **2017**, *7*, 365. [[CrossRef](#)]
11. Babu, N.J.; Sanphui, P.; Nangia, K. Crystal engineering of stable temozolomide cocrystals. *Chem.—Asian J.* **2012**, *7*, 2274–2285. [[CrossRef](#)] [[PubMed](#)]
12. Espinosa-Lara, J.C.; Guzman-Villanueva, D.; Arenas-García, J.I.; Herrera-Ruiz, D.; Rivera-Islas, J.; Román-Bravo, P.; Morales-Rojas, H.; Höpfl, H. Cocrystals of active pharmaceutical ingredients—Praziquantel in combination with oxalic, malonic, succinic, maleic, fumaric, glutaric, adipic, and pimelic acids. *Cryst. Growth Des.* **2012**, *13*, 169–185. [[CrossRef](#)]
13. Basavoju, S.; Bostrom, D.; Velaga, S.P. Pharmaceutical cocrystal and salts of norfloxacin. *Cryst. Growth Des.* **2006**, *12*, 2699–2708. [[CrossRef](#)]
14. Chen, J.M.; Wang, Z.Z.; Wu, C.B.; Li, S.; Lu, T.B. Crystal engineering approach to improve the solubility of mebendazole. *CrystEngComm* **2012**, *14*, 6221–6229. [[CrossRef](#)]
15. Wang, J.R.; Ye, C.; Zhu, B.; Mei, X. Pharmaceutical cocrystals of the anti-tuberculosis drug pyrazinamide with dicarboxylic and tricarboxylic acids. *CrystEngComm* **2015**, *17*, 747–752. [[CrossRef](#)]
16. Chen, G.; Højer, A.M.; Areberg, J.; Nomikos, G. Vortioxetine: Clinical pharmacokinetics and drug interactions. *Clin. Pharmacokinet.* **2018**, *57*, 673–686. [[CrossRef](#)] [[PubMed](#)]
17. He, S.F.; Zhang, X.R.; Zhang, S.; Guan, S.; Li, J.; Li, S.; Zhang, L. An investigation into vortioxetine salts: Crystal structure, thermal stability, and solubilization. *J. Pharm. Sci.* **2016**, *105*, 2123–2128. [[CrossRef](#)] [[PubMed](#)]
18. Li, J.; Li, L.Y.; He, S.F.; Li, S.; Dong, C.Z.; Zhang, L. Crystal structures, X-ray photoelectron spectroscopy, thermodynamic stabilities, and improved solubilities of 2-hydrochloride salts of vortioxetine. *J. Pharm. Sci.* **2017**, *106*, 1069–1074. [[CrossRef](#)] [[PubMed](#)]
19. Zhou, X.; Hu, X.; Wu, S.; Ye, J.; Sun, M.; Gu, J.; Zhu, J.; Zhang, Z. Structures and physicochemical properties of vortioxetine salts. *Acta Crystallogr. B* **2016**, *72*, 723–732. [[CrossRef](#)] [[PubMed](#)]
20. Zhang, S.; Zhang, X.R.; He, S.F.; Li, J.; Zhang, L. Syntheses, crystal structures and theoretical studies of three novel salts of vortioxetine and the investigation of their solubility. *Chin. J. Struct. Chem.* **2016**, *35*, 1645–1654.
21. Sheldrick, G.M. *Program for Empirical Absorption Correction of Area Detector Data*; University of Göttingen: Göttingen, Germany, 1996.
22. Sheldrick, G.M. *SHELXTL*, version 5.1; Bruker Analytical X-ray Instruments Inc.: Madison, WI, USA, 1998.
23. Sheldrick, G.M. *SHELXL-97*, PC version; University of Göttingen: Göttingen, Germany, 1997.

24. Suresh, K.; Nangia, A. Lornoxicam salts: Crystal structures, conformations, and solubility. *Cryst. Growth Des.* **2014**, *14*, 2945–2953. [[CrossRef](#)]
25. Swapna, B.; Maddileti, D.; Nangia, A. Cocrystals of the tuberculosis drug Isoniazid: Polymorphism, isostructurality, and stability. *Cryst. Growth Des.* **2014**, *14*, 5991–6005. [[CrossRef](#)]
26. Nangia, A. Conformational polymorphism in organic crystals. *Acc. Chem. Res.* **2008**, *41*, 595–604. [[CrossRef](#)] [[PubMed](#)]
27. Yalkowsky, S.H.; He, Y.; Jain, P. *Handbook of Aqueous Solubility Data*, 2nd ed.; CRC Press: Boca Raton, FL, USA, 2010.



© 2018 by the authors. Licensee MDPI, Basel, Switzerland. This article is an open access article distributed under the terms and conditions of the Creative Commons Attribution (CC BY) license (<http://creativecommons.org/licenses/by/4.0/>).